nature climate change

Article

https://doi.org/10.1038/s41558-024-02066-3

Asymmetries in the Southern Ocean contribution to global heat and carbon uptake

Received: 10 November 2023

Accepted: 13 June 2024

Published online: 24 July 2024

Check for updates

Richard G. Williams [1] ✉, Andrew J. S. Meijers [2], Vassil M. Roussenov [1], Anna Katavouta [3], Paulo Ceppi [4], Jonathan P. Rosser [2,5] & Pietro Salvi [6]

The Southern Ocean provides dominant contributions to global ocean heat and carbon uptake, which is widely interpreted as resulting from its unique upwelling and circulation. Here we show a large asymmetry in these contributions, with the Southern Ocean accounting for 83 ± 33% of global heat uptake versus 43 ± 3% of global ocean carbon uptake over the historical period in state-of-the-art climate models. Using single radiative forcing experiments, we demonstrate that this historical asymmetry is due to suppressed heat uptake by northern oceans from enhanced aerosol forcing. In future projections, such as SSP2-4.5 where greenhouse gases increasingly dominate radiative forcing, the Southern Ocean contributions to global heat and carbon uptake become more comparable, 52 ± 5% and 47 ± 4%, respectively. Hence, the past is not a reliable indicator of the future, with the northern oceans becoming important for heat uptake while the Southern Ocean remains important for both heat and carbon uptake.

The Southern Ocean plays a key role in the climate system by upwelling deep waters to the surface[1] and by ventilating the ocean through the formation of mode, intermediate and bottom waters[2,3]. Air–sea exchange acts to equilibrate the surface waters so that the upwelling of cold, old waters leads to an enhanced Southern Ocean uptake of excess heat and carbon from the atmosphere[4,5]. This enhanced Southern Ocean uptake does not lead to a proportionally large increase in Southern Ocean heat and carbon storage owing to redistribution by overturning circulations to the rest of the global ocean. The overturning circulation provides a northward transport of heat and anthropogenic carbon over the upper ocean, so that regions of enhanced ocean heat storage are downstream of the regions of enhanced air–sea heat uptake in the Southern Ocean[4] and there is a delay in climatically driven surface warming in the Southern Ocean[6].

This crucial role of the Southern Ocean in sequestering heat and carbon is highlighted in analyses of a suite of Earth system models from the Coupled Model Intercomparison Project phase 5 (CMIP5) integrated over the historical period from 1861 to 2005, revealing that the Southern Ocean accounted for 75 ± 22% of the heat uptake and 43 ± 3% of the carbon uptake by the global ocean over the historical period[7]. This disproportionately important role of the Southern Ocean in the global climate system is in keeping with its unique contribution to the upwelling of deep waters and ventilation of the global ocean.

A dominant role of the Southern Ocean for surface heat uptake is expected given the nature of the physical circulation, involving surface warming of upwelled cold water and subsequent redistribution of heat by a combination of the overturning and gyre circulations. However, it remains unclear why the Southern Ocean is not similarly important for carbon uptake. A priori, ventilation pathways of heat and carbon are expected to be broadly similar over the global ocean[8–12], so that the Southern Ocean contribution to global heat and carbon uptake might be expected to be similarly dominant.

[1]Department of Earth, Ocean and Ecological Sciences, School of Environmental Sciences, University of Liverpool, Liverpool, UK. [2]Polar Oceans, British Antarctic Survey, Cambridge, UK. [3]Marine Systems Modelling, National Oceanography Centre, Liverpool, UK. [4]Department of Physics, Imperial College London, London, UK. [5]Department of Applied Mathematics and Theoretical Physics, University of Cambridge, Cambridge, UK. [6]Institute for Atmospheric and Climate Science, ETH Zurich, Zurich, Switzerland. ✉e-mail: ric@liverpool.ac.uk

There are several possible explanations for this discrepancy. First, ocean uptake of heat from the atmosphere is influenced by radiative forcing and climate feedbacks[13], while the ocean uptake of carbon from the atmosphere is instead affected by carbonate-chemistry feedbacks[14–16] and a lesser extent by biological processes, which may lead to different regional responses. Second, the redistribution of anthropogenic heat and carbon may differ due to the regional contrasts in pre-industrial temperature being much larger and opposite in sign to those of dissolved inorganic carbon[17,18], which may lead to opposite-signed upper ocean heat and carbon anomalies. Thus, the relatively enhanced Southern Ocean uptake of heat compared with carbon might possibly be viewed as being due to differences in thermal and carbon processes and/or ocean redistribution for heat and carbon.

Notwithstanding the differences in heat and carbon cycling described above, here we propose a simpler explanation for the discrepancy in Southern Ocean heat and carbon uptake in terms of the hemispheric differences in radiative forcing. We diagnose the response of Coupled Model Intercomparison Project phase 6 (CMIP6) projections over the historical period, including experiments with single-component radiative forcings, and explore how this response differs for future projections up to year 2100 following the Shared Socioeconomic Pathway (SSP)2-4.5 scenario.

Historical Southern Ocean contribution

Over the historical period, the Southern Ocean (defined here, as in ref. 7, as south of 30° S) provides the dominant contribution to the global uptake of heat (Fig. 1a, left), accounting for 83 ± 33% of the rise in global ocean heat content between the decades of 1851–1860 and 2005–2014 on the basis of the multi-model, single-ensemble mean of 17 CMIP6 models (Table 1, list of models in Table 2 and individual responses in Supplementary Table 1). There is a large inter-model range in the Southern Ocean contribution. The rise in Southern Ocean heat uptake is relatively consistent between these two periods for these models, providing a model mean and standard deviation for the time-integrated surface heat uptake of $30 \pm 6 \times 10^{22}$ J. However, there is a corresponding wide range of model responses over the northern oceans for the surface heat uptake, $-6 \pm 16 \times 10^{22}$ J between these two periods, ranging from a strong heat loss to a modest heat uptake, leading to a northern ocean contribution of −17 ± 50% to the global ocean heat uptake (Supplementary Table 1). This hemispheric difference leads to the Southern Ocean heat uptake being comparable to the global ocean heat uptake of $36 \pm 18 \times 10^{22}$ J between these two periods. Hence, the large inter-model variability in the fraction of global heat uptake provided by the Southern Ocean is primarily due to the variability in the heat uptake by the northern oceans. While there is internal variability in the Earth system responses, the individual model ensembles all reveal that the Southern Ocean plays a more dominant role in heat uptake than the northern oceans (Supplementary Fig. 1a).

Turning to carbon uptake, we find that the Southern Ocean again provides a dominant contribution (Fig. 1a, right; 54 ± 5 Pg C; Supplementary Table 2), accounting for 43 ± 3% of the rise in global ocean uptake between the decade of 1851–1860 and 2005–2014 based on a multi-model, single-ensemble mean of 20 CMIP6 models (Table 1). In this case, the northern oceans consistently provide an uptake of carbon (26 ± 4 Pg C; Supplementary Table 2) accounting for 21 ± 2% of the global ocean carbon uptake. Hence, there is a much smaller range in the Southern Ocean or northern oceans contributions to the global ocean uptake of carbon compared with those for heat uptake. These CMIP6 results are broadly comparable to analyses of CMIP5 Earth system models[7].

The relative importance of the Southern Ocean in sequestering heat and carbon is highlighted here by comparing their fractional contributions with the global ocean uptake: the ratio of the fraction of global uptake provided by the Southern Ocean for heat versus carbon typically varies from 1.7 to 1.9 across the suite of models over the historical period (Table 1). Hence, the Southern Ocean is disproportionately important in sequestering heat as opposed to carbon over the historical period.

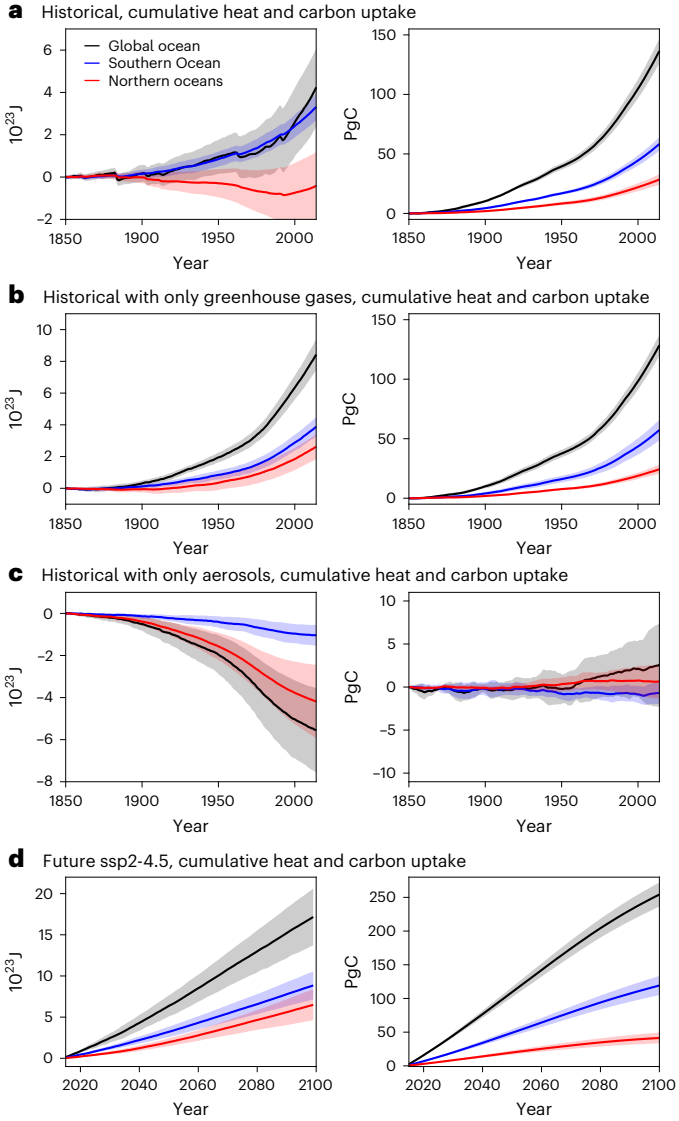

Fig. 1 | Transient evolution of cumulative heat and carbon uptake. a–d, The global (black line), northern ocean (red line) and Southern Ocean (blue line) uptakes for heat (left column) and carbon (right) over the historical period from 1850 to 2014 including all forcings (17 CMIP6 multi-model, single-ensemble means for heat and 20 CMIP6 multi-model, single-ensemble means for carbon) (**a**), single radiative forcing experiments over the historical period with either only greenhouse gases (**b**) or aerosols (five CMIP6 models with ensemble means for heat and five models with single ensembles for carbon) (**c**) and future projections following the SSP2-4.5 scenario from 2015 to 2100 from a subset of CMIP6 models (10 for heat and 17 for carbon) (**d**). The model mean and standard deviation are denoted by the lines and shading, and northern oceans and Southern Ocean domains defined as north of 30° N and south of 30° S, respectively.

We now explore the role of atmospheric heat sources involving regional differences in radiative forcing as a candidate driver for the asymmetry in how important the Southern Ocean is in contributing to the global uptake of heat and carbon.

Sensitivity of ocean heat uptake

The radiative forcing involves competing warming effects from greenhouse gases and cooling effects from aerosols. The aerosol forcing includes a direct effect involving the scattering and absorption of

Table 1 | Southern Ocean and northern ocean contributions towards global ocean uptake of heat and carbon

Earth system models	Period	Global ocean heat uptake by Southern Ocean (%)	Global ocean carbon uptake by Southern Ocean (%)	Ratio of the percentage of global heat uptake and carbon uptake by Southern Ocean	Global ocean heat uptake by northern oceans (%)	Global ocean carbon uptake by northern oceans (%)	Ratio of the percentage of global heat uptake and carbon uptake by northern oceans
(1) Historical experiments							
CMIP6, 17 models for heat, 20 for carbon	1851–1860 to 2005–2014	83±33%	43±3%	1.9	−17±50%	21±2%	−0.8
CMIP5 (ref. 7), 19 models	1861–1880 to 1986–2005	75±22%	43±3%	1.7	10%	22%	0.45
(2) Single radiative forcing experiments over the historical period with only greenhouse gases							
CMIP6, 5 models for heat and 5 for carbon	1851–1860 to 2005–2014	45±5%	45±4%	1.0	36±12%	19±2%	1.9
(3) Future projections for SSP2-4.5							
CMIP6, 10 models for heat and 17 for carbon	2015- 2024 to 2091–2100	52±7%	47±4%	1.11	38±8%	16±2%	2.4
(4) Idealized projection following a 1% annual increase in atmospheric CO_2							
CMIP6 (ref. 22), 12 models for heat and 11 for carbon	Years 121 to 140	44±5%	47±2%	0.94	–	–	–

Percentage contributions for: (1) the historical period; (2) for single radiative forcing experiments with only greenhouse gas forcing over the historical period; (3) future projections following SSP2-4.5; and (4) idealized projections following an annual 1% increase in atmospheric CO_2.

shortwave radiation, and indirect effects altering cloud albedo and cloud lifetime[19]. Over the historical period, there are large hemispheric contrasts in radiative forcing[20,21]: cooling from aerosols effectively offsets the warming from greenhouse gases over much of the Northern Hemisphere[19], while this effect from aerosols is more limited over the Southern Hemisphere. Therefore, most of the global supply of anomalous radiative heat to the surface occurs over the Southern Hemisphere[20,21].

Correspondingly, over the historical period, the hemispheric contrast in ocean heat uptake is consistent with the contrast in the planetary heat uptake at the top of the atmosphere (Fig. 2a, left). There is heat gain over the latitudes of the Southern Ocean (90–30° S) for the surface and top of the atmosphere, compared with a heat loss over the latitudes of the northern oceans (30–90° N). In contrast, the carbon uptake is more comparable between hemispheres (Fig. 2a, right), so it does not reveal the hemispheric asymmetry seen for heat uptake. This analysis is consistent with the prior CMIP5 analysis of ref. 7; see Supplementary Fig. 2 for the same historical time periods used in that analysis, 1861–1880 to 1986–2005.

To quantify the dependence of the fractional heat and carbon uptake by the Southern Ocean on the nature of the radiative forcing, we now examine CMIP6 experiments with single radiative forcing, where the radiative forcing is based either on historical greenhouse gas changes or historical non-greenhouse changes in aerosols. The greenhouse gases are assumed to be well mixed and ozone is fixed in time in the troposphere and stratosphere.

When the radiative forcing only consists of greenhouse gases, the northern and Southern oceans provide a comparable contribution to the global uptake of heat (Fig. 1b and Supplementary Fig. 1b for individual model ensembles) with an accompanying heat uptake at the top of the atmosphere over the latitudes of the northern oceans (30–90° N), based on analyses of five CMIP6 models (Fig. 2b). Hence, if there is only greenhouse gas forcing, the Southern Ocean proportion of global heat uptake decreases to 45 ± 5% and becomes effectively the same as its proportion of global ocean carbon uptake of 45 ± 4% (Table 1b and Extended Data Fig. 1a,b). In contrast, when the radiative forcing is only from aerosols, there is a marked Northern Hemisphere heat loss (see Figs. 1c and 2c and Supplementary Fig. 1c for individual model ensembles).

The different choices of radiative forcing affect the ocean redistribution of heat, as well as the ocean uptake of heat. The model-mean ocean heat transport at 30° N changes from being northward ($14 \pm 18 \times 10^{22}$ J) over the historical period for all forcings, supplying heat to the northern oceans, to weakly southward ($-10 \pm 15 \times 10^{22}$ J) for only greenhouse gas forcing and more strongly northward ($32 \pm 13 \times 10^{22}$ J) for only aerosol forcing (Fig. 2a–c).

These contrasting thermal responses may be understood from the model-mean patterns in the temporal change in the radiative forcing, F, and the planetary heat uptake at the top of the atmosphere, N (Methods), and their connection to the surface heat flux into the ocean. For the historical case with both greenhouse gas and aerosol forcing, F reaches 3 W m^{-2} over the tropics (directed into the ocean), but decreases to −3 W m^{-2} over parts of the Northern Hemisphere (Fig. 3a). The resulting heat uptake at the top of the atmosphere, N, is broadly similar to F—positive over the tropics and negative over parts of the Northern Hemisphere—but is enhanced by climate feedback over the latitudes of the Southern Ocean by typically 2 W m^{-2}. This climate feedback is also revealed in Earth system model diagnostics for an idealized scenario of an annual increase of 1% atmospheric CO_2, where the climate feedback is due to a positive albedo feedback[22] from a reduction in sea ice.

The temporal change in the model-mean surface ocean heat input reaches 10 W m^{-2} and is enhanced over much of the Southern Ocean together with localized regions of heat input over the eastern tropical Pacific and the subpolar North Atlantic and North Pacific. In contrast, the temporal change in the model-mean surface flux of CO_2 is directed into the ocean over most of the Southern Ocean and more extensively over the high latitude regions of the North Atlantic and North Pacific. The inter-model spread in surface heat and carbon uptake by the ocean is greatest over the North Atlantic and Southern Ocean (Supplementary Fig. 3).

For the historical case with only greenhouse gas forcing, the radiative forcing F becomes positive over the entire globe with enhanced values over the tropics and slightly weaker values over the high latitudes (Fig. 3b). In turn, the heat uptake at the top of the atmosphere N becomes more symmetric across both hemispheres in this case, reflecting the pattern of radiative forcing, and again includes an enhancement in planetary heat uptake from climate feedback over the latitudes of the Southern Ocean. The surface heat flux into the ocean remains large into the Southern Ocean, but increases in the north, especially over the subpolar North Atlantic.

https://doi.org/10.1038/s41558-024-02066-3

Table 2 | List of CMIP6 models used for the different diagnostics in this study

Historical scenario	Historical heat	Historical carbon	Historical radiative forcing agent experiments for heat: greenhouse gas or aerosol forcings	Historical radiative forcing agent experiments for carbon: greenhouse gas or aerosol forcings	SSP2-4.5 heat projection	SSP2-4.5 carbon projection	Reference
ACCESS-CM2	Y		Y		Y		Bi et al.[33]
ACCESS-ESM1-5	Y	Y		Y		Y	Ziehn et al.[34]
CAMS-CSM1-0	Y				Y		Zhou et al.[35]
CanESM5	Y	Y	Y (9 ensembles)	Y	Y	Y	Swart et al.[36]
CanESM5-CanOE	Y	Y			Y	Y	
CESM2	Y	Y		Y		Y	Danabasoglu et al.[37]
CESM2-WACCM	Y	Y			Y	Y	
CIESM	Y						Lin et al.[38]
CMCC-ESM2		Y				Y	Lovato et al.[39]
CNRM-CM6-1			Y		Y		Voldoire et al.[40]
CNRM-ESM2-1	Y	Y			Y	Y	Séférian et al.[41]
EC-Earth3	Y						Döscher et al.[42]
EC-Earth3-CC		Y				Y	Döscher et al.[42]
FIO-ESM-2-0	Y						Bao et al.[43]
GFDL-ESM4	Y	Y			Y	Y	Dunne et al.[44]
GISS-E2-1-G		Y					Kelley et al.[45]
HadGEM3-GC31-LL	Y		Y (5 ensembles)				Roberts et al.[46]
IPSL-CM6A-LR		Y	Y (9 ensembles)	Y		Y	Boucher et al.[47]
IPSL-CM5A1-INCA		Y					Sepulchre et al.[48]
MIROC-ES2H		Y				Y	Kawamiya et al.[49]
MIROC-ES2L		Y				Y	Hajima et al.[50]
MPI-ESM1-2-LR	Y	Y				Y	Mauritsen et al.[51]
MPI-ESM1-2-HR	Y	Y			Y	Y	
MRI-ESM2-0	Y	Y					Yukimoto et al.[52]
NorESM2-LM		Y		Y		Y	Seland et al.[53]
NorESM2-MM		Y				Y	Seland et al.[53]
UKESM1-0-LL	Y	Y			Y	Y	Sellar et al.[54]
Number of CMIP6 models used for each analysis	17	20	5 (25 ensembles)	5	10	17	

CMIP6, Coupled Model Intercomparison Project phase 6; SSP, Shared Socio-economic Pathway.

For the historical case with only aerosol forcing, the radiative forcing F instead becomes negative (Fig. 3c), especially over the Northern Hemisphere. This negative F drives a heat loss at the top of the atmosphere over much of the globe with only a weak heat input over parts of the Southern Hemisphere. The surface heat flux into the ocean becomes negative over much of the surface ocean with a pronounced surface heat loss over the subpolar North Atlantic, reflecting the hemispheric bias in aerosol distribution[19].

In summary, the single radiative forcing experiments endorse the view that over the historical period, the hemispheric contrasts in radiative forcing are primarily due to aerosol forcing[19–21], acting to offset and oppose the heat input at the top of the atmosphere by greenhouse gases over the Northern Hemisphere, while only having a limited effect over the Southern Hemisphere. Climate feedbacks[13,22,23] act to weakly enhance the heat input over the latitudes of the Southern Ocean. The radiative responses at the top of the atmosphere then lead to hemispheric contrasts in the area-integrated surface heat flux into the ocean. The surface heat flux is directed into the ocean over the Southern Hemisphere, especially over the Southern Ocean, and is instead directed out of the ocean over parts of the northern oceans. The strength and sign of the surface heat loss over the northern oceans varies with the radiative forcing and the contribution of aerosols (Figs. 2a–c and 3a–c). There is not the same hemispheric asymmetry in the ocean carbon uptake. Hence, the hemispheric contrasts in radiative forcing over the historical period give rise to the asymmetry between the patterns of ocean heat and carbon uptake, which in turn lead to the Southern Ocean providing a much more dominant contribution to global ocean uptake of heat than carbon.

Southern Ocean future response

Next, we consider what the future might hold for the role of the Southern Ocean in sequestering heat and carbon over the global ocean. Following the 'middle-of-the-road' SSP2-4.5, both the Southern Ocean and northern oceans make important contributions to how heat is sequestered by the end of the century. For this scenario, the radiative forcing from aerosols decreases in magnitude from −0.6 W m^{-2} at year 2020 to −0.2 W m^{-2} at year 2100[24].

The radiative forcing, F, is much more evenly distributed from the increasing greenhouse gases in SSP2-4.5 and is projected to reach 6 W m^{-2} over much of the globe (Fig. 3d). The heat flux at the top of the

https://doi.org/10.1038/s41558-024-02066-3

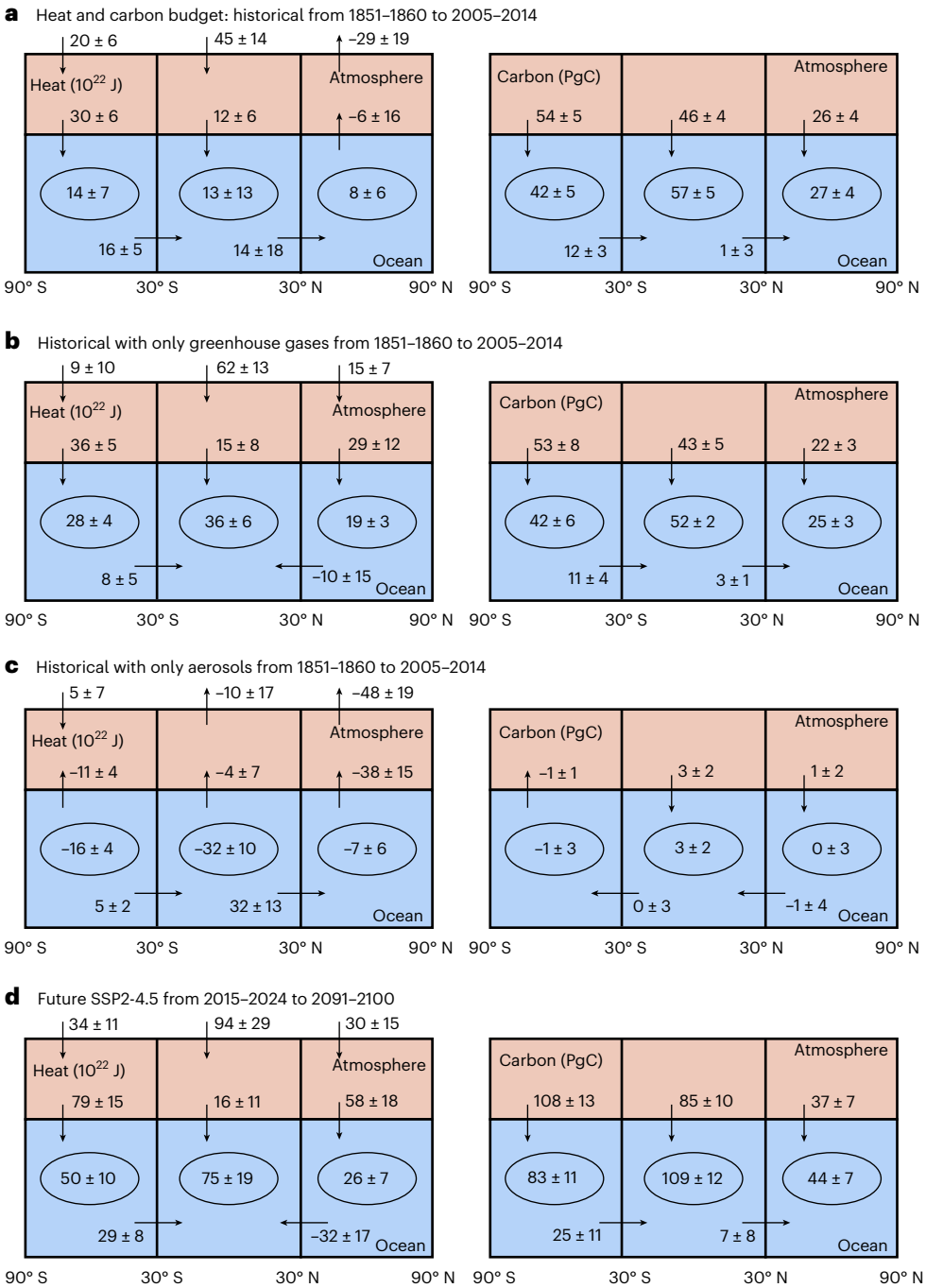

Fig. 2 | Historical and future changes in the cumulative fluxes and storage of heat and carbon. a–**d**, The historical changes in heat (left) and carbon (right) for all radiative forcings and single radiative forcing experiments (**a**) only including the effects of greenhouse gases (**b**) or aerosols (**c**), compared with future projected changes following SSP2-4.5 (**d**). The cumulative changes in **a**–**c** are for a recent decade 2005–2014 relative to a decade in the pre-industrial era 1851–1860 and for **d** for 2091–2100 relative to 2015–2024, which are evaluated for the top of the atmosphere, the surface ocean and the ocean interior, and implied transports through latitudes of 30° N and 30° S. Diagnostics are based on 17 CMIP6 multi-model, single-ensemble means for heat and 20 CMIP6 multi-model, single-ensemble means for carbon (**a**); 5 CMIP6 models with ensemble means for heat and single ensembles for carbon (**b** and **c**); and 10 CMIP6 multi-model, single-ensemble means for heat and 17 for carbon (**d**).

atmosphere, N, reaches 6 W m^{-2} over the tropical Pacific and 2–3 W m^{-2} over the latitudes of the Southern Ocean. This future pattern in heat uptake at the top of the atmosphere is consistent with the future pattern in surface heat uptake strengthening and becoming more symmetric between the hemisphere (Fig. 3d), compared with the historical cases.

Accordingly, in the projections, the Southern Ocean (Figs. 1d and 2d) reduces its proportion of global heat uptake to 52 ± 7% in the multi-model, single-ensemble mean, while the Northern Hemisphere contribution increases to 38 ± 8% (Table 1c, Supplementary Table 1 for 10 CMIP6 models and Supplementary Fig. 3a,c). The heat transport at 30° N changes to being directed southward rather than northward as in the historical period (Fig. 2d).

The global contribution of the Southern Ocean to global heat uptake, 52 ± 7%, is now much more comparable to its contribution to global ocean carbon uptake of 47 ± 4%, based on a multi-model,

https://doi.org/10.1038/s41558-024-02066-3

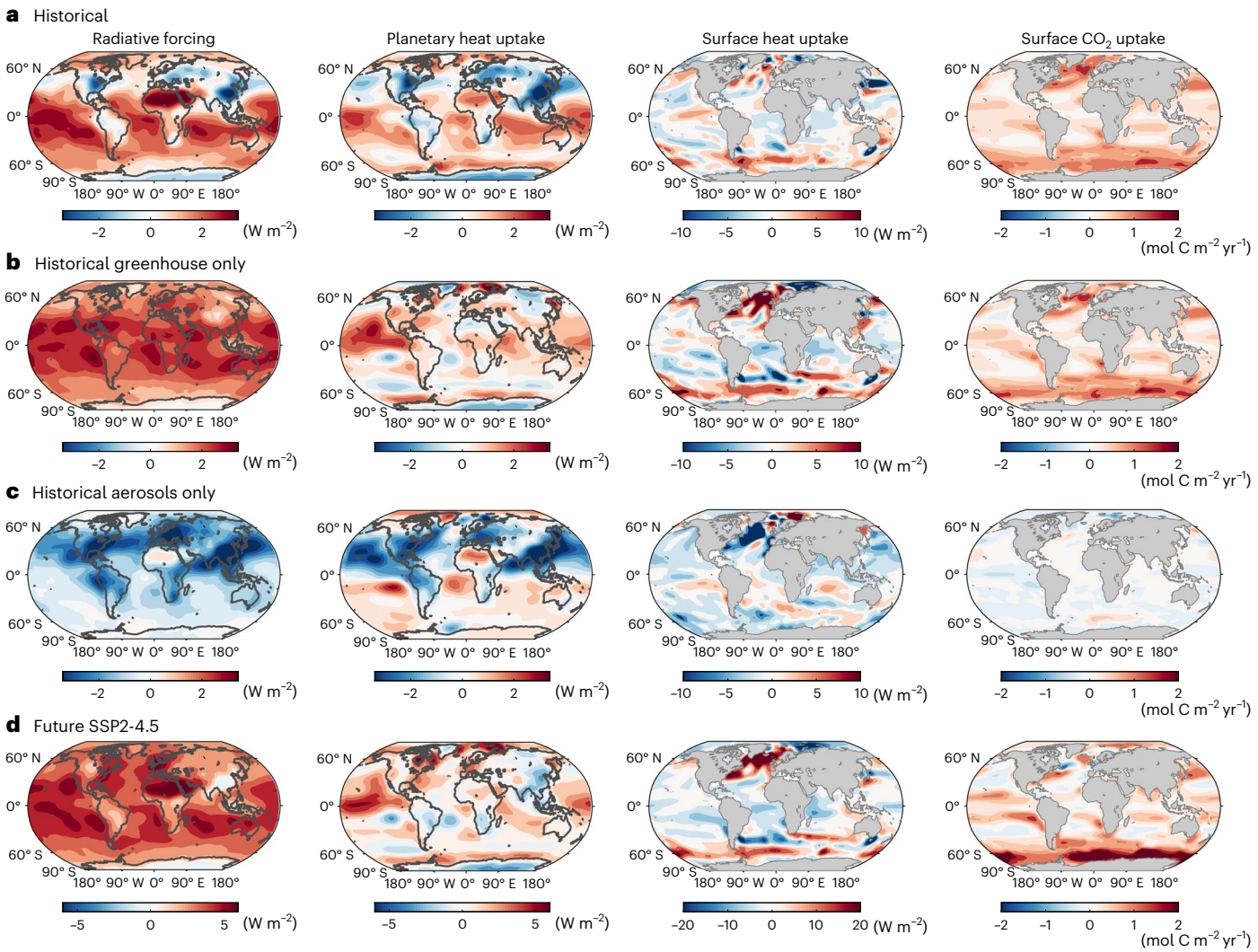

Fig. 3 | Historical and future changes in radiative forcing and heat and carbon uptake. a–d, Maps of the temporal change in the radiative forcing at the top of the atmosphere (W m^{-2}), planetary heat uptake (W m^{-2}), surface ocean heat uptake (W m^{-2}) and surface ocean CO_2 uptake (mol C m^{-2} yr^{-1}) evaluated for the historical period for all forcings (**a**), single radiative forcing experiments including only the effects of greenhouse gases (**b**) or aerosols (**c**) and compared with future projections following SSP2-4.5 (shown with an increased range for the radiative and thermal fluxes) (**d**). The maps in **a**–**c** are for a recent decade 2005–2014 relative to a decade in the pre-industrial era 1851–1860 and for **d** for 2091–2100 relative to 1851–1860. Diagnostics are based on model means: 17 CMIP6 multi-model, single-ensemble means for heat, 20 CMIP6 multi-model, single-ensemble means for carbon (**a**); 5 CMIP6 models with ensemble means for heat and single ensembles for carbon (**b** and **c**); and 10 CMIP6 multi-model, single-ensemble means for heat and 17 for carbon (**d**). Accompanying standard deviations are shown in Supplementary Fig. 3.

single-ensemble mean of 17 CMIP6 models (Fig. 1d, Table 1c and Extended Data Figs. 1a,c and 2 relative to the pre-industrial era).

There is a future projected slight decrease in the effectiveness of the northern oceans in sequestering carbon, dropping from 21 ± 2% over the historical period to 16 ± 2% for the SSP2 scenario (Extended Data Fig. 1a,c). This reduction mainly involves a decrease over the North Atlantic. This relative weakening in carbon uptake in the northern oceans is partly offset by an increase in the northward transport of carbon from the Southern Ocean and the tropics (Fig. 2d).

This change in character of how the Southern Ocean and northern oceans contribute to the global heat and carbon uptake is demonstrated in scatter plots for the individual Earth system models (Fig. 4a,b), revealing the much greater Southern Ocean contribution to global heat uptake for the historical period compared with a more comparable contribution to global heat uptake and carbon uptake in the future (see model-mean time-varying responses in Fig. 4c,d). This more comparable role of the Southern Ocean for heat and carbon is also evident for an idealized scenario of a 1% annual increase in atmospheric CO_2, which demonstrates a Southern Ocean contribution south of 30° S of 44 ± 5% for heat uptake and 47 ± 2% for carbon uptake[23] (Table 1 and Supplementary Table 3 for 11 CMIP6 models).

Discussion

Over the historical period, the Southern Ocean has played a more important role than the northern oceans in how heat is sequestered relative to carbon. There has typically been nearly twice as large a contribution of the Southern Ocean to heat uptake than carbon uptake for the global ocean. While there are unique upwelling and overturning circulations occurring in the Southern Ocean, our analysis suggests that the primary reason for the enhanced Southern Ocean uptake of heat relative to carbon are differences in their atmospheric sources. Over the historical period, there are strong hemispheric contrasts in radiative forcing, with non-greenhouse gas radiative forcing from aerosols providing a cooling over much of the Northern Hemisphere, competing with the greenhouse gas forcing providing a warming over both hemispheres[19–21]. Thus, the net radiative forcing

https://doi.org/10.1038/s41558-024-02066-3

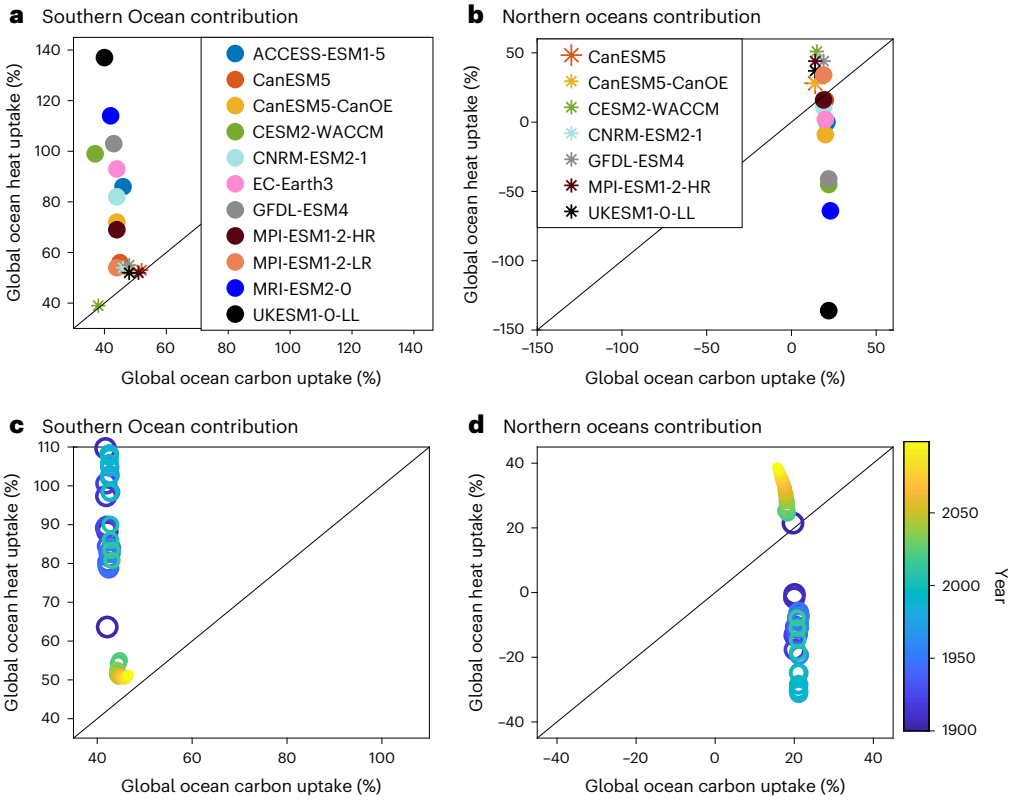

Fig. 4 | Southern and northern ocean contributions to global uptake compared for heat and carbon. a,**b**, Individual model responses for the percentages of global heat versus global carbon uptake occurring over the Southern Ocean (**a**) or northern ocean (**b**) for recent historical period 2005–2014 (circles) and for future projections for the period 2091–2100 following the SSP2-4.5 scenario (stars). **c**,**d**, Model-mean, time-varying contributions for the percentages of global heat versus global carbon uptake occurring over the Southern Ocean (**c**) and the northern oceans (**d**), which are colour coded in time from year 1900 (blue) onwards to year 2100 (yellow). Diagnostics are based on 11 CMIP6 models for the historical period and 7 CMIP6 models for the future period to 2100. The Southern Ocean historically provides a larger contribution to global heat uptake compared with carbon uptake, whereas its contributions to global heat and carbon uptake become more comparable to future projections following SSP2-4.5.

providing the overall heat input into the global ocean is preferentially occurring over the Southern Ocean[25,26]. In contrast, the atmospheric CO_2 source occurs more evenly over both hemispheres, providing a more comparable input over both the northern oceans and the Southern Ocean. For idealized scenario experiments that only include radiative forcing from greenhouse gases, the Southern Ocean likewise provides very similar global ocean contributions to the uptake of heat and carbon[22].

The historical asymmetry in radiative forcing does not lead to large hemispheric differences in ocean heat storage (Fig. 2), as is also seen in observations, such as the similar hemispheric sea level change records[26]. Instead, the regional effect of aerosol cooling[19–21] has been partly offset by a strengthening in the ocean overturning[26–29] and the resulting redistribution of heat. There are notable inter-model differences in the Earth system model responses, particularly for the thermal responses. There are a range of reasons for these differences: model differences in the treatment of non-CO_2 radiative forcing agents, particularly aerosols and their indirect cloud effects[19,28]; the representation of climate feedbacks, particularly involving clouds and sea ice[13,23]; and differences in the strength of the ocean overturning[26–29], acting to redistribute heat and carbon.

The dominance of the Southern Ocean over the historical period for global heat uptake relative to carbon uptake is likely to alter in the future, as radiative forcing from greenhouse gases increasingly dominates[24] and aerosol forcing weakens[28]. This change in radiative forcing alters the ocean redistribution of heat: the multi-model mean for the ocean heat transport at 30° N is northward over the historical period, offsetting a surface heat loss over the northern oceans, and changes sign to southward for the future SSP2-4.5 scenario, redistributing a surface heat gain over the northern oceans (Fig. 2a,d).

For future scenarios, following either a plausible choice of SSP2-4.5 or an idealized annual 1% increase in atmospheric CO_2, the Southern Ocean provides a much more comparable contribution to the global ocean uptake of heat and carbon, consistent with the northern oceans becoming important in sequestering heat as well as carbon. The shift from Northern Hemisphere heat loss towards a gain is evident even in historical scenarios where the heat loss progressively reduces from the mid-1980s onward. This response is evident in other CMIP6 analyses of Northern Hemisphere heat uptake[30,31] and is probably related to the reduction in aerosol concentrations following emission control efforts[32].

Our findings may be generalized to emphasize the importance of atmospheric sources of heat and carbon in determining the global efficiency of ocean heat and carbon uptake, which is at the heart of uncertainties in climate projections. For example, in a scenario where the sources are concentrated in the high latitudes, a greater fraction of that excess heat or carbon may be taken up by the ocean (because the high latitudes are efficient at taking up heat or carbon), whereas in a scenario where the sources are focused on the tropics, the fraction of excess heat or carbon taken up by the ocean may be less.

Finally, the past response of the ocean in the climate system might not be a reliable indicator of its future role, as differences in the past and future patterns in radiative forcing affect which ocean ventilation regions are important in how heat is sequestered compared with how carbon is sequestered. This finding challenges the widely held view of the unique Southern Ocean overturning circulation being the linchpin

of global ocean warming, instead suggesting that its importance is currently exacerbated due to hemispheric biases in surface heating, and that its role in future warming will be reduced relative to that of the rest of the global ocean.

Online content

Any methods, additional references, Nature Portfolio reporting summaries, source data, extended data, supplementary information, acknowledgements, peer review information; details of author contributions and competing interests; and statements of data and code availability are available at https://doi.org/10.1038/s41558-024-02066-3.

References

1. Morrison, A. K., Frölicher, T. L. & Sarmiento, J. L. Upwelling in the Southern Ocean. *Phys. Today* **68**, 27 (2015).
2. Sallée, J. B., Speer, K., Rintoul, S. & Wijffels, S. Southern Ocean thermocline ventilation. *J. Phys. Oceanogr.* **40**, 509–529 (2010).
3. Marshall, J. & Speer, K. Closure of the meridional overturning circulation through Southern Ocean upwelling. *Nat. Geosci.* **5**, 171–180 (2012).
4. Marshall, J. et al. The ocean's role in the transient response of climate to abrupt greenhouse gas forcing. *Clim. Dyn.* **44**, 2287–2299 (2015).
5. Gruber, N., Landschützer, P. & Lovenduski, N. S. The variable Southern Ocean carbon sink. *Annu. Rev. Mar. Sci.* **11**, 159–186 (2019).
6. Armour, K. C., Marshall, J., Scott, J. R., Donohoe, A. & Newsom, E. R. Southern Ocean warming delayed by circumpolar upwelling and equatorward transport. *Nat. Geosci.* **9**, 549–554 (2016).
7. Frölicher, T. L. et al. Dominance of the Southern Ocean in anthropogenic carbon and heat uptake in CMIP5 models. *J. Clim.* **28**, 862–886 (2015).
8. Haine, T. W. & Hall, T. M. A generalized transport theory: water-mass composition and age. *J. Phys. Oceanogr.* **32**, 1932–1946 (2002).
9. Waugh, D. W., Hall, T. M., McNeil, B. I., Key, R. & Matear, R. J. Anthropogenic CO_2 in the oceans estimated using transit time distributions. *Tellus B* **58**, 376–389 (2006).
10. Goodwin, P., Williams, R. G. & Ridgwell, A. Sensitivity of climate to cumulative carbon emissions due to compensation of ocean heat and carbon uptake. *Nat. Geosci.* **8**, 29–34 (2015).
11. Bronselaer, B. & Zanna, L. Heat and carbon coupling reveals ocean warming due to circulation changes. *Nature* **584**, 227–233 (2020).
12. Bourgeois, T., Goris, N., Schwinger, J. & Tjiputra, J. F. Stratification constrains future heat and carbon uptake in the Southern Ocean between 30° S and 55° S. *Nat. Commun.* **13**, 340 (2022).
13. Sherwood, S. C. et al. An assessment of Earth's climate sensitivity using multiple lines of evidence. *Rev. Geophys.* **58**, e2019RG000678 (2020).
14. Gregory, J. M., Jones, C. D., Cadule, P. & Friedlingstein, P. Quantifying carbon cycle feedbacks. *J. Clim.* **22**, 5232–5250 (2009).
15. Arora, V. K. et al. Carbon concentration and carbon–climate feedbacks in CMIP6 models and their comparison to CMIP5 models. *Biogeosciences* **17**, 4173–4222 (2020).
16. Katavouta, A. & Williams, R. G. Ocean carbon cycle feedbacks in CMIP6 models: contributions from different basins. *Biogeosciences* **18**, 3189–3218 (2021).
17. Winton, M., Griffies, S. M., Samuels, B. L., Sarmiento, J. L. & Frölicher, T. L. Connecting changing ocean circulation with changing climate. *J. Clim.* **26**, 2268–2278 (2013).
18. Williams, R. G., Katavouta, A. & Roussenov, V. Regional asymmetries in ocean heat and carbon storage due to dynamic redistribution in climate model projections. *J. Clim.* **34**, 3907–3925 (2021).
19. Booth, B. B., Dunstone, N. J., Halloran, P. R., Andrews, T. & Bellouin, N. Aerosols implicated as a prime driver of twentieth-century North Atlantic climate variability. *Nature* **484**, 228–232 (2012).
20. Cai, W. et al. Pan-oceanic response to increasing anthropogenic aerosols: impacts on the Southern Hemisphere oceanic circulation. *Geophys. Res. Lett.* **33**, L21707 (2006).
21. Wang, H. & Wen, Y. J. Climate response to the spatial and temporal evolutions of anthropogenic aerosol forcing. *Clim. Dyn.* **59**, 1579–1595 (2022).
22. Williams, R. G., Ceppi., P., Roussenov, V., Katavouta, A. & Meijers, A. The role of the Southern Ocean in the global climate response to carbon emissions. *Philisoph. Trans. A* https://doi.org/10.1098/rsta.2022.0062 (2023).
23. Zelinka, M. D. et al. Causes of higher climate sensitivity in CMIP6 models. *Geophys. Res. Lett.* **47**, e2019GL085782 (2020).
24. Lund, M. T., Myhre, G. & Samset, B. H. Anthropogenic aerosol forcing under the Shared Socioeconomic Pathways. *Atmos. Chem. Phys.* **19**, 13827–13839 (2019).
25. Shi, J. R., Xie, S. P. & Talley, L. D. Evolving relative importance of the Southern Ocean and North Atlantic in anthropogenic ocean heat uptake. *J. Clim.* **31**, 7459–7479 (2018).
26. Irving, D., Wijffels, S. & Church, J. Anthropogenic aerosols, greenhouse gases, and the uptake, transport, and storage of excess heat in the climate system. *Geophys. Res. Lett.* **46**, 4894–4903 (2019).
27. Menary, M. B. et al. Aerosol-forced AMOC changes in CMIP6 historical simulations. *Geophys. Res. Lett.* **47**, e2020GL088166 (2020).
28. Ma, X., Liu, W., Allen, R. J., Huang, G. & Li, X. Dependence of regional ocean heat uptake on anthropogenic warming scenarios. *Sci. Adv.* **6**, eabc0303 (2020).
29. Robson, J. et al. The role of anthropogenic aerosol forcing in the 1850–1985 strengthening of the AMOC in CMIP6 historical simulations. *J. Clim.* **35**, 6843–6863 (2022).
30. Li, S., Liu, W., Allen, R. J., Shi, J. R. & Li, L. Ocean heat uptake and interbasin redistribution driven by anthropogenic aerosols and greenhouse gases. *Nat. Geosci.* **16**, 695–703 (2023).
31. Shi, J. R., Wijffels, S. E., Kwon, Y. O., Talley, L. D. & Gille, S. T. The competition between anthropogenic aerosol and greenhouse gas climate forcing is revealed by North Pacific water-mass changes. *Sci. Adv.* **9**, eadh7746 (2023).
32. Quaas, J. et al. Robust evidence for reversal of the trend in aerosol effective climate forcing. *Atmos. Chem. Phys.* **22**, 12221–12239 (2022).
33. Bi, D. et al. Configuration and spin-up of ACCESS-CM2, the new generation Australian community climate and Earth System simulator coupled model. *J. South. Hemisph. Earth Syst. Sci.* **70**, 225–251 (2020).
34. Ziehn, T. et al. The Australian Earth system model: ACCESS-ESM1.5. *J. South. Hemisph. Earth Syst. Sci.* **70**, 193–214 (2020).
35. Zhou, T. et al. Development of climate and Earth system models in China: past achievements and new CMIP6 results. *J. Meteorol. Res.* **34**, 1–19 (2020).
36. Swart, N. C. et al. The Canadian Earth system model version 5 (CanESM5. 0.3). *Geosci. Model Dev.* **12**, 4823–4873 (2019).
37. Danabasoglu, G. et al. The community Earth system model version 2 (CESM2). *J. Adv. Model. Earth Syst.* **12**, e2019MS001916 (2020).
38. Lin, Y. et al. Community integrated Earth system model (CIESM): description and evaluation. *J. Adv. Model. Earth Syst.* **12**, e2019MS002036 (2020).
39. Lovato, T. et al. CMIP6 simulations with the CMCC Earth system Model (CMCC-ESM2). *J. Adv. Model. Earth Syst.* **14**, e2021MS002814 (2022).

40. Voldoire, A. et al. Evaluation of CMIP6 deck experiments with CNRM-CM6-1. *J. Adv. Model. Earth Syst.* **11**, 2177–2213 (2019).
41. Séférian, R. et al. Evaluation of CNRM Earth system model, CNRM-ESM2-1: role of Earth system processes in present-day and future climate. *J. Adv. Model. Earth Syst.* **11**, 4182–4227 (2019).
42. Döscher, R. et al. The EC-earth3 Earth system model for the climate model intercomparison project 6. *Geosci. Model Dev. Discuss.* **2021**, 1–90 (2021).
43. Bao, Y., Song, Z. & Qiao, F. FIO-ESM version 2.0: model description and evaluation. *J. Geophys. Res. Oceans* **125**, e2019JC016036 (2020).
44. Dunne, J. P. et al. The GFDL Earth system model version 4.1 (GFDL-ESM 4.1): overall coupled model description and simulation characteristics. *J. Adv. Model. Earth Syst.* **12**, e2019MS002015 (2020).
45. Kelley, M. et al. GISS-E2. 1: configurations and climatology. *J. Adv. Model. Earth Syst.* **12**, e2019MS002025 (2020).
46. Roberts, M. J. et al. Description of the resolution hierarchy of the global coupled HadGEM3-GC3. 1 model as used in CMIP6 HighResMIP experiments. *Geosci. Model Dev.* **12**, 4999–5028 (2019).
47. Boucher, O. et al. Presentation and evaluation of the IPSL-CM6A-LR climate model. *J. Adv. Model. Earth Syst.* **12**, e2019MS002010 (2020).
48. Sepulchre, P. et al. IPSL-CM5A2—an Earth system model designed for multi-millennial climate simulations. *Geosci. Model Dev.* **13**, 3011–3053 (2020).
49. Kawamiya, M. et al. Two decades of Earth system modeling with an emphasis on Model for Interdisciplinary Research on Climate (MIROC). *Prog. Earth Planet Sci.* **7**, 64 (2020).
50. Hajima, T. et al. Development of the MIROC-ES2L Earth system model and the evaluation of biogeochemical processes and feedbacks. *Geosci. Model Dev.* **13**, 2197–2244 (2020).
51. Mauritsen, T. et al. Developments in the MPI-M Earth system model version 1.2 (MPI-ESM1. 2) and its response to increasing CO_2. *J. Adv. Model. Earth Syst.* **11**, 998–1038 (2019).
52. Yukimoto, S. et al. The Meteorological Research Institute Earth system model version 2.0, MRI-ESM2. 0: description and basic evaluation of the physical component. *J. Meteorol. Soc. Jpn. Ser. II* **97**, 931–965 (2019).
53. Seland, Ø. et al. Overview of the Norwegian Earth system model (NorESM2) and key climate response of CMIP6 DECK, historical, and scenario simulations. *Geosci. Model Dev.* **13**, 6165–6200 (2020).
54. Sellar, A. A. et al. UKESM1: description and evaluation of the UK Earth system model. *J. Adv. Model. Earth Syst.* **11**, 4513–4558 (2019).

Methods

The role of the Southern Ocean in determining the global climate response to historical radiative forcing, including the effect of greenhouse gases affected by carbon emissions and non-greenhouse gas forcing from aerosols, is assessed following the CMIP6 experiments over the historical period. Different subsets of the CMIP6 models are utilized depending on the data archived and model experiments performed (Table 2). The surface warming and top-of-the-atmosphere heat balance are diagnosed using a multi-model, single-ensemble mean from 17 CMIP6 models and the ocean carbon uptake using a multi-model, single-ensemble mean from 20 CMIP6 models. Experiments with different radiative forcing are conducted with a smaller subset of five CMIP6 models due to limited data availability, but are based on ensemble means (Table 2). When multiple ensembles are available for a given model run, these are first averaged together before calculating heat content and heat uptake (Supplementary Information 2). The global and regional values are calculated as area integrals over the globe or over the region south of 30° S for the Southern Ocean or over the region to the north of 30° N for the northern oceans.

For all model variables, the underlying model drift is corrected for by subtracting the parallel pre-industrial control integration, where there is no external forcing (that is, no greenhouse nor aerosol emissions and associated radiative forcing).

The mean and standard deviations of the percentage contribution[55] that a region makes to global uptake is evaluated from the model mean, standard deviation and correlation for the regional uptake, A, and global uptake, B: the model mean of the ratio is taken from $\hat{A}/\hat{B}$ where $\hat{A}$ and $\hat{B}$ are their model means; and the standard deviation of the ratio is taken from $\sigma_{A/B} = \left|\frac{\hat{A}}{\hat{B}}\right|\left(\left(\frac{\sigma_A}{\hat{A}}\right)^2 + \left(\frac{\sigma_B}{\hat{B}}\right)^2 - \frac{2\rho_{AB}\sigma_A\sigma_B}{\hat{A}\hat{B}}\right)^{\frac{1}{2}}$ where σ_A and σ_B are the model standard deviations for A and B, and ρ_{AB} is the model correlation between A and B.

Definitions of heat and carbon uptake

Heat and carbon uptake is evaluated from the time integral of the air–sea heat and carbon fluxes over a particular time period. This ocean heat and carbon uptake, linking to changes in ocean heat and carbon content over that time period, may be viewed in terms of an input of anthropogenic heat and CO_2 from the atmosphere plus a feedback due to changes in the natural climate system. In this study, we do not separate these different anthropogenic and feedback contributions, as this separation requires additional model integrations; see ref. 56 for heat and ref. 15 for carbon.

Ocean heat uptake and storage

The cumulative ocean heat uptake, Q_{uptake} in J, over a time period from time t_0 is evaluated as

$$Q_{\text{uptake}}(r,t) = \int_{t_0}^{t}\int_{A} H_{\text{net}}(r,t)\,\mathrm{d}A\mathrm{d}t, \tag{1}$$

where $H_{\text{net}}(r,t)$ is the surface heat flux (positive into ocean) in W m^{-2} from all sources (CMIP6 variable hfds), A is the ocean surface area, r and t denote space and time indices, respectively, and t_0 is a reference time period. Individual model responses are presented in Supplementary Table 1.

The ocean heat content, Q_{storage} in J, relative to that at a reference time at t_0 is evaluated over a volume integral

$$Q_{\text{storage}}(r,t) = \rho_0 C_{\text{p}}\int_{V}(\theta(r,t) - \theta(r,t_0))\mathrm{d}V, \tag{2}$$

where ρ_0 is the potential density (assumed here to be a constant value of 1,024 kg m^{-3}), C_{p} is the specific heat capacity (assumed to be a constant of 4,000 J kg^{-1} K^{-1}), θ is the ocean potential temperature, dV is the volume element and the integral is performed over the volume V.

The ocean heat storage and the surface heat flux are evaluated on the native model grid. These analyses are then binned by latitude and summed zonally to provide the area-integrated surface heat flux in equation (1) or summed both zonally and with depth to provide area-integrated estimates of the change in ocean heat storage in equation (2). There are small mismatches between the global volume integrated heat content change and the area-integrated surface heat flux due to how the datasets have been evaluated, either binned monthly or evaluated online.

The northward ocean heat transport across 30° S and 30° N is diagnosed from a heat budget on the basis of the residual from the mismatch between the change in the ocean heat storage from equation (2) and the air–sea heat flux integrated south and north of these latitudes respectively from equation (1).

Radiative diagnostics

The time-evolving top-of-the-atmosphere radiative energy budget is evaluated as

$$N(r,t) = \Delta F(r,t) + \Delta R(r,t), \tag{3}$$

where N is the net heat input at the top of the atmosphere, ΔF is the increase in radiative forcing and ΔR is the radiative response, representing a change in radiative heat loss to space. All fluxes are in W m^{-2} and all positive values represent a planetary heat input. N is simply the net heat imbalance from the difference between the net absorbed shortwave radiation and the outgoing longwave radiation, directly obtained from monthly climate model output.

The multi-model mean of the area-integrated and time-integrated heat flux over the historical period (1851–1860 to 2005–2014) at the top of the atmosphere, $36 \pm 17 \times 10^{22}$ J, is close to the area-integrated and time-integrated global surface ocean heat uptake, $36 \pm 18 \times 10^{22}$ J, with a multi-model mean and standard deviation of their ratios given by 100 ± 14% (Supplementary Tables 1 and 3).

There is a large inter-model spread in the model means with mismatches greater than 20% for ACCESS-CM2, CESM2, CNRM-ESM2-1, HadGEM3-GC31-LL and UKESM1-0-LL; in these cases, there are large surface heat losses over the Northern Hemisphere and relatively small global surface heat uptakes. The global heat balance is improved in the future projections, reaching a multi-model mean and standard deviation of 97 ± 6% for the SSP2-4.5 scenario (Supplementary Table 3). Individual models generally have a misfit of less than 10% in the energy balance.

Carbon content diagnostics

The cumulative ocean carbon uptake, C_{uptake} in gC, is estimated as

$$C_{\text{uptake}}(r,t) = \int_{A}\int_{t_0}^{t} F_{\text{carbon}}(r,t)\,\mathrm{d}t\mathrm{d}A, \tag{4}$$

where F_{carbon} is the air–sea flux of carbon into the ocean in gC m^{-2} s^{-1} over a surface area A and t_0 is a reference time period. Individual model responses are presented in Supplementary Table 2.

The global ocean carbon storage, C_{storage} in gC, relative to a reference time period at time t_0 is estimated from a volumetric integral of the dissolved inorganic carbon

$$C_{\text{storage}}(r,t) = c\int_{V}(\text{DIC}(r,t) - \text{DIC}(r,t_0))\mathrm{d}V, \tag{5}$$

where DIC is the dissolved inorganic carbon in mol C m^{-3} and $c = 12.01$ g mol^{-1} is a converting factor from moles to grams of carbon and the integral is performed over the volume V. When integrated over

the global ocean, the ocean carbon uptake and ocean carbon storage are equivalent, except from a small contribution from carbon flux from river run-off and the carbon burial in ocean sediments.

The northward ocean carbon transport across 30° S and 30° N is diagnosed from a carbon budget on the basis of the residual from the mismatch between the change in the ocean carbon storage from equation (5) and the air–sea carbon flux integrated south and north of these latitudes respectively from equation (4).

Data availability

The data used here are from the CMIP6 simulations performed by the various modelling groups and available from the Earth System Grid Federation at the CMIP6 archive (https://esgf-node.llnl.gov/search/cmip6, World Climate Research Programme, 2021). The processed data employed for this study is available at ref. 57.

References

55. Lee, E. S. & Forthofer, R. N. *Analyzing Complex Survey Data* (SAGE Publications, 2006).
56. Gregory, J. M. et al. The Flux-Anomaly-Forced Model Intercomparison Project (FAFMIP) contribution to CMIP6: investigation of sea-level and ocean climate change in response to CO_2 forcing. *Geosci. Model Dev.* **9**, 3993–4017 (2016).
57. Roussenov, V. et al. Asymmetries in the Southern Ocean contribution to global heat and carbon uptake. *Zenodo* https://doi.org/10.5281/zenodo.11397243 (2024).

Acknowledgements

The authors acknowledge the World Climate Research Programme, which, through its Working Group on Coupled Modelling, coordinated and promoted CMIP6; the climate modelling groups for producing and making available their model output; and the Earth System Grid Federation for archiving the data and providing access. Surface heat fluxes and ocean heat storage calculations were performed using the Pangeo platform. We thank B. Booth for helpful comments. There are no competing interests. This research was supported by grants from the UK Natural Environment Research Council: NE/T007788/1 (R.G.W., P.C., V.M.R. and A.K.); NE/T010657/1 (SARDINE) (R.G.W. and V.M.R.); NE/W009501/1 (C-Streams) (R.G.W. and V.M.R.); NE/T006250/1 (P.C.); NE/T01069X/1 (SARDINE) (A.J.S.M.), NE/N018095/1 (ORCHESTRA) (A.J.S.M.), NE/V013254/1 (ENCORE) (A.J.S.M.) and NE/W004933/1 (BIOPOLE) (A.J.S.M.); and NE/S007164/1 (J.P.R.); and European Union Horizon 2020 101003536 (S.P.).

Author contributions

R.G.W., A.J.S.M., P.C., A.K. and V.M.R. jointly conceived the study. A.J.S.M. and J.P.R. provided the ocean heat data from CMIP6 models. P.C. and P.S. provided the top-of-the-atmosphere radiative flux data. A.K. provided and analysed the carbon data from CMIP6 models. V.M.R. analysed the thermal data and together with A.K. provided the figures and tables. R.G.W. wrote the first draft of the paper. All authors contributed to the writing and proofreading.

Competing interests

The authors declare no competing interests.

Additional information

Extended data is available for this paper at https://doi.org/10.1038/s41558-024-02066-3.

Supplementary information The online version contains supplementary material available at https://doi.org/10.1038/s41558-024-02066-3.

Correspondence and requests for materials should be addressed to Richard G. Williams.

Peer review information *Nature Climate Change* thanks Timothée Bourgeois, Weiwei Fu and the other, anonymous, reviewer(s) for their contribution to the peer review of this work.

https://doi.org/10.1038/s41558-024-02066-3

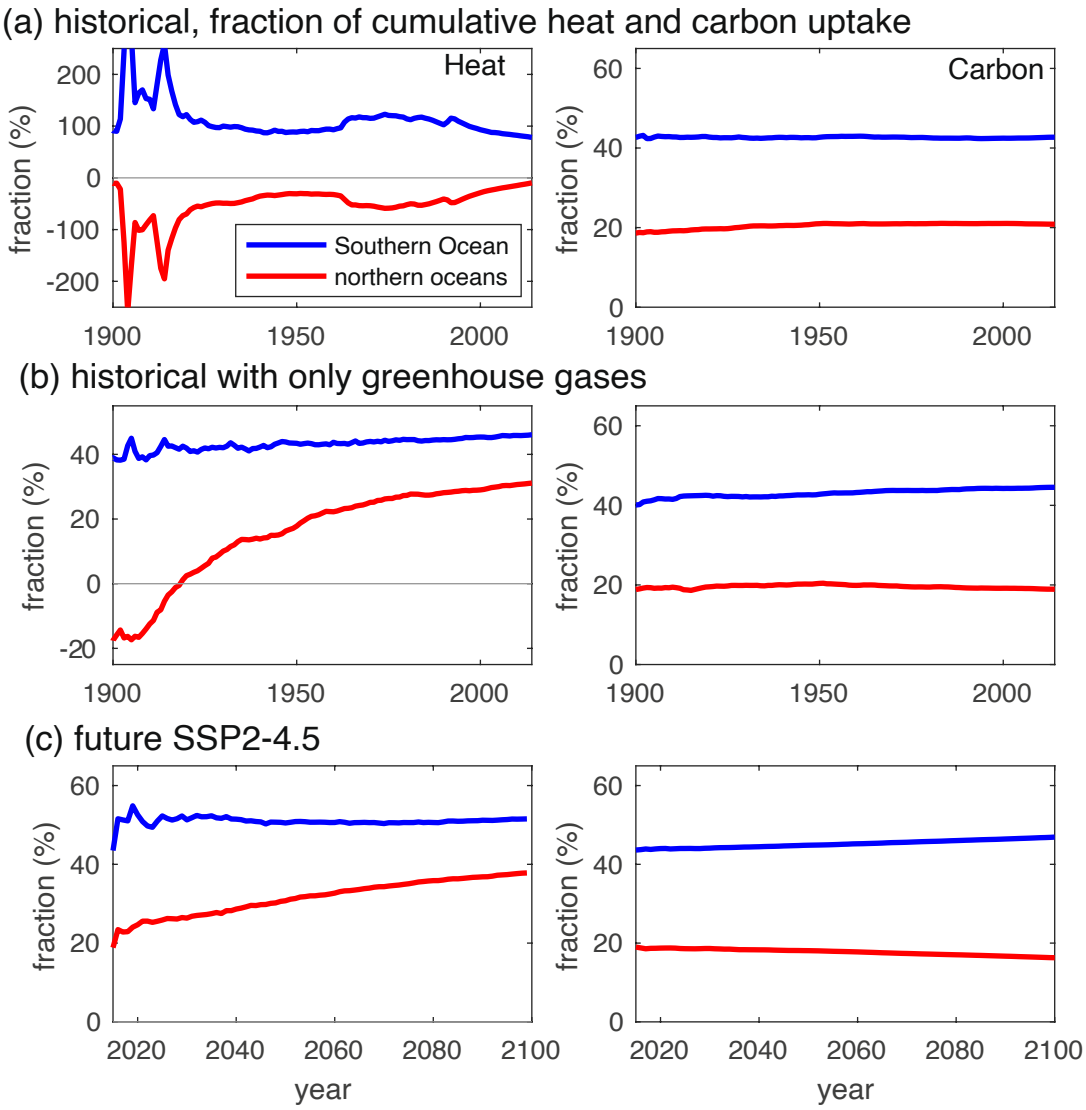

Extended Data Fig. 1 | Historical and future time-varying contributions to global cumulative heat and carbon uptake. Time-varying contributions of the Southern Ocean (blue line) and northern oceans (red line) for global heat uptake (left panel) and global carbon uptake (right panel): (**a**) historical period for all forcing relative to 1851 to 1860 shown from years 1900 to 2020, (**b**) the historical period for single radiative forcing from greenhouse gases; and (**c**) future shared socio-economic pathway SSP2–4.5 from years 2015 to 2100 relative to 2015 to 2024. These percentages over their last decade are consistent with those shown in Supplementary Tables 1 and 2. Diagnostics are based on model-mean responses for: (a) 17 CMIP6 multi-model, single-ensemble means for heat, 20 CMIP6 multi-model, single-ensemble means for carbon; (b) 5 CMIP6 models with ensemble means for heat and single ensembles for carbon; and (c) 10 CMIP6 multi-model, single-ensemble means for heat and 17 for carbon.

https://doi.org/10.1038/s41558-024-02066-3

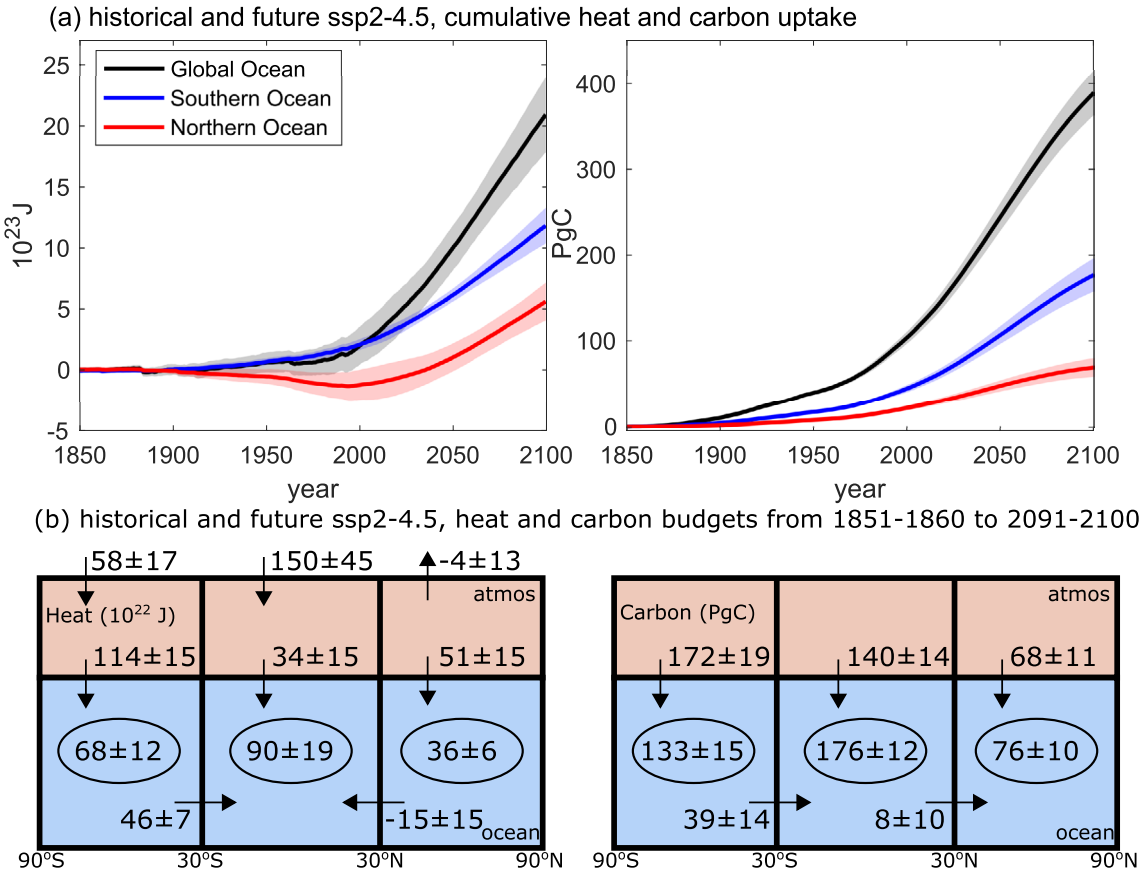

Extended Data Fig. 2 | Historical and future cumulative heat and carbon uptake. Combined historical and future projection for heat and carbon uptake: (**a**) Transient evolution of global (black line), northern oceans (red line) and southern oceans (blue line) for heat and carbon following the shared socio-economic pathway SSP2-4.5 scenario from 1850 to 2100; (**b**) synthesis plot for the change in the cumulative fluxes and storage of heat and carbon for 2091 to 2100 relative to 1861 to 1880, which are evaluated for the top of the atmosphere, the surface ocean and the ocean interior, and implied transports through latitudes of 30°N and 30°S. In (a) there is the model mean and standard deviation (shading) with northern and southern ocean domains defined as north of 30°N and south of 30°S respectively. Diagnostics are based on 10 CMIP6 multi-model, single-ensemble means for heat and 17 CMIP6 multi-model, single-ensemble means for carbon.